HHS Public Access

Author manuscript

Brain Imaging Behav. Author manuscript; available in PMC 2016 June 01.

Published in final edited form as:

Brain Imaging Behav. 2015 June ; 9(2): 342–352. doi:10.1007/s11682-014-9314-z.

Multi-Tensor Investigation of Orbitofrontal Cortex Tracts Affected in Subcaudate Tractotomy

Jimmy C. Yang, B.A.[2,5], **George Papadimitriou, B.S.**[1], **Ryan Eckbo, B.S., M.Sc.**[4], **Edward H. Yeterian, Ph.D.**[6], **Lichen Liang, Ph.D.**[1], **Darin D. Dougherty, M.D., M.Sc.**[3,5], **Sylvain Bouix, Ph.D.**[4,5], **Yogesh Rathi, Ph.D.**[4,5], **Martha Shenton, Ph.D.**[4,5,7], **Marek Kubicki, M.D., Ph.D.**[4,5], **Emad N. Eskandar, M.D.**[2,5,*], and **Nikos Makris, M.D., Ph.D.**[1,5,*]

[1]Departments of Psychiatry and Neurology, Center for Morphometric Analysis, A. Martinos Center for Biomedical Imaging, Massachusetts General Hospital, Boston, MA, USA

[2]Department of Neurosurgery, Massachusetts General Hospital, Boston, MA, USA

[3]Department of Psychiatry, Massachusetts General Hospital, Boston, MA, USA

[4]Department of Psychiatry, Psychiatry Neuroimaging Laboratory, Brigham and Women's Hospital, Boston, MA, USA

[5]Harvard Medical School, Boston, MA, USA

[6]Department of Psychology, Colby College, Waterville, ME, USA

[7]VA Boston Healthcare System, Brockton, MA, USA

Abstract

Subcaudate tractotomy (SCT) is a neurosurgical lesioning procedure that can reduce symptoms in medically intractable obsessive compulsive disorder (OCD). Due to the putative importance the orbitofrontal cortex (OFC) in symptomatology, fibers that connect the OFC, SCT lesion, and either the thalamus or brainstem were investigated with two-tensor tractography using an unscented Kalman filter approach. From this dataset, fibers were warped to Montreal Neurological Institute space, and probability maps with center-of-mass analysis were subsequently generated.

In comparing fibers from the same OFC region, including medial OFC (mOFC), central OFC (cOFC), and lateral OFC (lOFC), the area of divergence for fibers connected with the thalamus versus the brainstem is posterior to the anterior commissure. At the anterior commissure, fibers connected with the thalamus run dorsal to those connected with the brainstem. As OFC fibers travel through the ventral aspect of the internal capsule, lOFC fibers are dorsal to cOFC and

Corresponding author: Nikos Makris, M.D., Ph.D., Departments of Psychiatry and Neurology Services, Center for Morphometric Analysis, Athinoula A. Martinos Center for Biomedical Imaging, Massachusetts General Hospital, Building 149, 13th Street, Charlestown, MA 02129, (617) 726-5743, nikos@cma.mgh.harvard.edu.

*These authors contributed equally to this work

Disclosures: All authors confirm adherence to ethical research standards and report no conflicts of interest or personal commercial or financial interest in any of the materials or devices described

Informed Consent

All procedures followed were in accordance with the ethical standards of the responsible committee on human experimentation (institutional and national) and with the Helsinki Declaration of 1975, as revised in 2000 (5). Informed consent was obtained from all patients for being included in the study.

mOFC fibers. Using neuroanatomical comparison, tracts coursing between the OFC and thalamus are likely part of the anterior thalamic radiations, while those between the OFC and brainstem likely belong to the medial forebrain bundle. These data support the involvement of the OFC in OCD and may be relevant to creating differential lesional procedures of specific tracts or to developing deep brain stimulation programming paradigms.

Keywords

psychosurgery; diffusion tensor imaging; diffusion tractography; obsessive-compulsive disorder; deep brain stimulation

Introduction

In cases of medically intractable psychiatric disease, neurosurgical treatment is an option for reducing symptom burden and increasing quality of life. Forty to sixty percent of patients with obsessive-compulsive disorder (OCD) do not have satisfactory response to optimal management (Pallanti and Quercioli 2006). As a result, neurosurgical techniques, which include stereotactic lesioning of specific areas of the brain involved in psychopathology, have been used for therapeutic benefit. Procedures currently used include anterior cingulotomy, subcaudate tractotomy, and, a combination of the two, called the limbic leucotomy (Kelly et al. 1973; Mashour et al. 2005).

Outcomes for these procedures have been largely positive. The most recent studies in OCD patients have shown that approximately 45% improve after cingulotomy (Dougherty et al. 2002; Jung et al. 2006) and 70% improve after subcaudate tractotomy (Bridges et al. 1994; Hodgkiss et al. 1995). At Massachusetts General Hospital, the limbic leucotomy is completed with a subcaudate tractotomy after non-response to anterior cingulotomy, and a recent study showed that 73% of these patients show symptom improvement (Bourne et al. 2013).

The target of the anterior cingulotomy is more anatomically homogenous, with the lesion directly targeting the cingulum bundle (Leiphart and Valone 2010). In contrast, the effects of subcaudate tractotomy, developed by Knight in 1960, are less clear; the lesion targets the white matter ventral to the head of the caudate nucleus to disrupt corticostriatothalamic pathways (Feldman et al. 2001; Knight 1969; Mashour et al. 2005). Previous work by our group studied the direct gray and white matter structures that are lesioned, which include the uncinate fasciculus, orbitofrontal cortex, and nucleus accumbens, but the disrupted connections between specific structures were not delineated (Yang et al., 2014).

Given the notable efficacy of SCT in cases of medically intractable OCD, an understanding of the disrupted connectivity may provide further insight into the neural substrates of OCD and provide guidance in making the SCT lesion more effective. In this study, we used multi-tensor based tractography in 60 normal subjects to delineate and to identify the anatomical connections between the medial, central, and lateral orbitofrontal cortex (OFC) and thalamus or brainstem that pass through the region affected by SCT.

Materials and Methods

Subjects

The initial dataset for this study involved healthy subjects with an average age of 34 and without diagnosed neurological disorder or drug dependency, with demographics described in a prior study (Makris et al. 2013). Informed consent was obtained from all subjects, and the study was IRB-approved.

MRI Acquisition

Description of MRI parameters is described in further detail in a prior study (Makris et al. 2013). A 3T GE Echospeed system (General Electric Medical Systems, Milwaukee, WI) was used to obtain T1-weighted and T2-weighted images, and diffusion data were collected with an echo planar imaging (EPI) HARDI pulse sequence.

Briefly, parameters are as follows: T1-weighted sequence: TR=7.4 ms, TE= 3 ms, TI=600, 100 flip angle, 25.6 cm^2 field of view, matrix=256×256, and voxel dimensions of 1×1×1 mm^3. T2-weighted sequence: TR=2,500 ms, TE=80 ms, 25.6 cm^2 field of view, and voxel dimensions 1×1×1 mm^3. EPI HARDI sequence: TR=17,000 ms, TE=78 ms, FOV=24 cm, 144×144 encoding steps with slice thickness=1.7 mm, resulting in isotropic 1.7×1.7×1.7 mm^3 voxels. A double echo sequence with an 8-channel coil and ASSET (Array Spatial Sensitivity Encoding Techniques, GE) was used. Ultimately, 51 noncollinear diffusion directions with b=900 s/mm^2 and eight baseline scans with b=0 s/mm^2 were acquired.

Diffusion Image Processing and Tractography

Diffusion images were corrected for motion and eddy currents by using FSL-based software (The Oxford Centre for Functional MRI of the Brain, University of Oxford, Oxford, UK).

Anatomic structures close to the OFC, such as bone and air-filled sinuses, result in magnetic field inhomogeneity that often causes distortion in diffusion data. As a result, using Advanced Normalization Tools (ANTs) (Avants et al. 2008), EPI distortion correction was performed via 1D deformable registration with mutual information metric of the b=0 s/mm^2 image to a rigidly aligned reference T2-weighted image (Ardekani and Sinha 2005). This method restricts the registration of the diffusion image onto the T2-weighted image such that the diffusion data may only be warped in the same direction as the phase encoding direction. Ultimately, 60 subjects from the original dataset were fully processed in preparation for tractography.

Two-tensor whole brain tractography was subsequently implemented with MATLAB using an algorithm that uses an unscented Kalman filter (Malcolm et al. 2010). This form of tractography involves a recursive process that both fits local parameters at each step and propagates the fiber in the most stable direction, allowing simultaneous tractography and model estimation. This model also uses a covariance matrix to measure confidence, which reduces false positives, and implements two eigenvalues per voxel, which improves resolution of and accounts for branching and crossing fibers. Whole-brain tractography was

used to best account for all potential tracts among the ROIs, which may be otherwise limited in solely ROI-based tractography.

Region of Interest (ROI) Delineation

The representative SCT lesion was delineated by using data from 11 subjects who had undergone a limbic leucotomy for medically intractable psychiatric diagnoses between 2001 and 2008. At our institution, the limbic leucotomy is carried out by adding the subcaudate tractotomy lesion after a prior anterior cingulotomy. Details of the subcaudate tractotomy lesion procedure can be found in a prior study (Yang et al. 2014).

T1-weighted images of subjects with SCT lesions were segmented in Freeview, which is part of the FreeSurfer imaging software package (Athinoula A. Martinos Center for Biomedical Imaging, Massachusetts General Hospital, Boston, MA, USA), and the resulting output was a volume mask (per subject). Since these lesion masks were delineated on clinical MR images (in native acquisition space), a linear, manual, landmark-based (anterior commissure, posterior commissure, and interhemispheric plane (Filipek et al. 1994; Talairach and Tournoux 1988)) registration with 12 degrees of freedom was used to register each subject to the Montreal Neurological Institute (MNI) MNI152 brain. As clinical MR images containing large lesions may cause automated methods to fail, and because clinical images may not be of the entire brain due to patient considerations, this approach was considered the most accurate. One author (JCY) performed the lesion segmentations, which were corroborated by a neuroanatomist (NM). To determine intra-rater reliability, re-segmentation on a subset of lesions was performed and Cronbach's alpha was calculated to identify volumetric and spatial reliability.

The representative SCT lesion was subsequently created by using FSLMaths, part of the FMRIB Software Library package. All registered lesion masks were added using FSLMaths and voxels that overlapped in 5 or more subjects were extracted to form the representative lesion. The average voxel size of all subjects was 13320 ± 686 voxels (standard error), and the representative SCT lesion was 13584 voxels.

ROI identification for medial OFC (mOFC), central OFC (cOFC), lateral OFC (lOFC), thalamus, and brainstem were isolated from the MNI152-based Massachusetts General Hospital-Center for Morphometric Analysis (CMA) structural atlas (Fig. 1) (Caviness et al. 1996; Makris et al. 1999; Meyer et al. 1999; Poellinger et al. 2001; Rademacher et al. 1992). Of note, the cOFC ROI was derived from combining the ROIs known as the anterior OFC (aOFC) and posterior OFC (pOFC) (Fig. 1). As many studies that have divided the OFC into different regions use the cOFC ROI rather than the aOFC and pOFC ROIs, this cOFC ROI definition allowed the resultant data to be best comparable to prior studies (Jbabdi et al. 2013; Lehman et al. 2011). Lehman *et al*. (2011) used a tracer approach to understanding connections from homologous ventral medial prefrontal cortex (vmPFC), mOFC, cOFC, and lOFC regions of the macaque, and Jbabdi *et al*. (2013) built upon this work by using probabilistic tractography with human and macaque diffusion that was seeded in discrete areas of the vmPFC, cOFC, and lOFC. Notable differences study's ROI delineation include the investigation of the mOFC region as well as utilization entire ROI for extracting fiber tracts from whole brain tractography analysis, rather than seed regions.

The SCT lesion was subsequently added to the CMA atlas, creating a complete MNI152-label map. Finally, the T1-weighted MNI152 brain was registered to the baseline DWI subject using ANTs, and the label map underwent the same deformation. These labels subsequently used to filter out fibers from the whole-brain tractography that traversed following ROI combinations: (1) mOFC-SCT-thalamus, (2) mOFC-SCT-brainstem, SCT-thalamus, (4) cOFC-SCT-brainstem, (5) lOFC-SCT-thalamus, and (6) lOFC-SCT146 brainstem.

Fiber Warping and Probability Maps

To create probability maps for tracts affected by the SCT lesion, the baseline DWI data subject was ultimately registered to the MNI152 template using ANTs. These deformations then applied to the fiber tracts to place all fibers in MNI152 space. Fiber tract masks created and averaged to obtain a probabilistic map, and maps were thresholded at 1.5% clarity. For each map, center-of-mass coordinates were subsequently obtained in each intersecting coronal plane, and coordinates were transformed to Talairach space.

Results

Data from a total of 60 subjects were corrected using a registration-based method, on which whole-brain tractography and fiber isolation were performed to delineate fibers that traversed mOFC or cOFC or lOFC, SCT lesion, and thalamus or brainstem. As described previously (Yang et al. 2014), creation of the SCT lesion, based on clinical MRI scans, had high intra-rater reliability, with the percent of overlapping voxels calculated to be 91% and with a Cronbach's alpha of 0.98 based on lesion volume.

Fibers connecting the mOFC, SCT, and thalamus were most commonly identified in this dataset, with mOFC-SCT-thalamus fibers identified on the right side in 86.7% of subjects and on the left side in 95% of subjects. lOFC-SCT-thalamus fibers were isolated on the right side in 56.7% and on the left side in 53.3% of subjects. Right mOFC-SCT-brainstem fibers were found in 55%, left mOFC-SCT-brainstem fibers in 63.3%, right lOFC-SCT-brainstem fibers in 53.3%, and left lOFC-SCT-brainstem fibers in 46.7% of subjects. For the relatively larger cOFC ROI, cOFC170 SCT-thalamus fibers were found in 100% of subjects, bilaterally. The cOFC-SCT-brainstem fiber was isolated in 88.3% of subjects on the right side and 95% of subjects on the left side.

Fibers coursing between the OFC and brainstem or thalamus, that were interrupted by the SCT lesion, were found to run in the internal capsule with a specific orientation (Fig. 2, Fig. 3). Tracts running from the lOFC travel dorsally to those from the cOFC, which are similarly dorsal to the mOFC. While mOFC and cOFC tracts to the thalamus additionally involved a white matter tract that traveled ventrolateral to the putamen in the external capsule, these fibers were not seen in mOFC, cOFC, or lOFC tracts to the brainstem (Fig. 3). In examining the mOFC, cOFC, and lOFC, fibers targeting the thalamus versus the brainstem diverged posterior to the anterior commissure (Fig. 2, Fig. 3).

The SCT lesions and each tract probability map was plotted by using a center-of-mass approach to generate Talairach coordinates (Makris et al. 2013) (Fig. 4, Fig. 5, Fig. 6,

Supplementary Table 1). These plots show similar findings to the probability maps, in which the fibers originating from the mOFC are ventral to those from the lOFC, with an area of tract divergence slightly anterior to the anterior commissure with fibers separating to target either the thalamus or brainstem (Fig. 4). At the level of the anterior commissure (the 0 mm position on the Talairach anterior-posterior axis), the fibers have a particular pattern in which those connected to the thalamus are dorsal to those connected to the brainstem. Probability maps of cOFC fibers demonstrated overlap with mOFC. However, using the center-of-mass approach, separate averaged tracts could be resolved and demonstrate that cOFC fibers to both the thalamus and brainstem follow similar organizing rules as the mOFC and lOFC, as cOFC fibers were found to travel between the mOFC and lOFC fibers (Fig. 4, Fig. 5, Fig. 6).

In visualizing the probability map projections and the SCT lesion, an understanding of the primarily affected tracts is made clear. Given their ventral position, mOFC tracts appear to be more significantly involved in the SCT lesion, as compared with the more dorsal lOFC tracts. Correspondingly, mOFC tracts were most affected by the dorsolateral portions of the SCT lesions.

Discussion

In this study, we used multi-tensor whole-brain tractography to isolate white matter tracts from the orbitofrontal cortex that are affected by subcaudate tractotomy (SCT). We show that tracts connecting the mOFC, cOFC and lOFC with the thalamus or brainstem are all affected by SCT and that these tracts have a particular topographic organization, in which tracts connecting the mOFC travel ventral to those connecting the lOFC, with cOFC fibers coursing in between. At the level of the anterior commissure, these fibers are organized such that those connected to the thalamus travel dorsally to those connected to the brainstem.

In order to reduce the possibility of having isolated false positives using this method of multi-tensor tractography, a neuroanatomical examination of these fibers, with comparison to atlases was conducted. Tracts that travel between the orbitofrontal cortex and thalamus are part of the anterior thalamic radiation and connect with the medial aspect of the thalamus (Fig. 5). Using approximate Talairach coordinates and an atlas-based approach (Talairach and Tournoux 1988), fibers from the lOFC were seen to connect to the mediodorsal nucleus (−20mm A-P axis, ±5mm M-L axis, 8mm I-S axis) while fibers from the mOFC terminate in the mediodorsal and pulvinar nuclei (-30mm A-P axis, ±15mm M-L axis, 10mm I-S axis). The OFC-SCT-brainstem pathways were localized to the dorsal aspect of the brainstem (Fig. 6), and these fibers are believed to be part of the medial forebrain bundle based on their location relative to the cerebral aqueduct and their trajectory through the brainstem and ventral diencephalon (Fig. 55 (Paxinos and Huang 1995); Fig. 191.13 (Nieuwenhuys et al. 1988); (Nieuwenhuys et al. 2008)) (Coenen et al. 2012; Coenen et al. 2011). The latter is a major pathway interconnecting the forebrain with the brainstem and is associated with limbic functions (Nieuwenhuys et al. 2008).

In addition, these fiber connections are further supported by primate tracer studies. The connection between the OFC and the pulvinar nucleus has been substantiated in a number of

studies (Barbas et al. 1991; Bos and Benevento 1975; Cavada et al. 2000; Kievit and Kuypers 1977; Romanski et al. 1997; Trojanowski and Jacobson 1976; Yeterian and Pandya 1988). In addition, the connections between the OFC and the mediodorsal nucleus (Barbas et al. 1991; Ray and Price 1993; Yeterian and Pandya 1988) and the OFC and the brainstem (An et al. 1998; Frankle et al. 2006; Porrino and Goldman-Rakic 1982) have been demonstrated. Overall, these primate anatomical studies support the OFC-SCT-thalamus and OFC-SCT-brainstem fibers elucidated in this study.

With the support of these anatomical data, the subcaudate tractotomy ROI used in this study provides further insight into the neuropathology underlying OCD. The neuropathobiology of OCD has been described in terms of the corticostriatothalamocortical (CSTC) circuit, which has been implicated in OCD (Bourne et al. 2012; Haber and Brucker 2009). Multiple studies have demonstrated that areas of cortex connected by the CSTC circuit can be anatomically and functionally different in disease states. For example, meta-analyses have shown that patients with OCD have reduced gray matter density in the dorsolateral prefrontal cortex (DLPFC) and OFC and reduced volume of the anterior cingulate cortex (ACC) and OFC (Rotge et al. 2009; Rotge et al. 2010a; Szeszko et al. 1999). In addition, fMRI and PET studies of OCD patients have shown that stimulus presentation activates the OFC, DLPFC, ACC, and basal ganglia (Adler et al. 2000; Braber et al. 2010; Breiter et al. 1996; McGuire et al. 1994; Rauch et al. 1994; Rotge et al. 2008). Notably, successful treatment of OCD by pharmacologic, behavioral, and neurosurgical methods reduces activity in this circuit (Baxter et al. 1992; Haber and Brucker 2009; Perani et al. 1995; Schwartz et al. 1996; Swedo et al. 1992).

The OFC has been of particular interest in the context of OCD given its activity under disease states that predict treatment response and because OFC morphometric abnormalities may offer insight into OCD pathophysiology (Greenberg et al. 2010; Piras et al. 2013). Studies have implicated aberrant OFC activity and connectivity in OCD (Beucke et al. 2013; Hou et al. 2012), and differential roles of the mOFC and lOFC are thought to play a role in OCD symptomatology, such as with delay discounting (Bari and Robbins 2013). While it remains unclear whether the mOFC or the lOFC plays a more significant role in disease, with both being implicated in recent studies (Hoexter et al. 2013; Rotge et al. 2010b), animal models have provided possible insight into disease processes *in vivo*. Recent studies have shown that stimulation of the OFC260 ventromedial striatum network can recapitulate an OCD phenotype in rodents, which further supports the role of CSTC dysregulation in OCD (Ahmari et al. 2013). Interestingly, in a separate study, simulation of lOFC and its terminals in the striatum in rodents led to a reduced OCD-like phenotype (Burguière et al. 2013).

In non-human primates, the medial-lateral organization of the OFC subdivisions use a particular route, aligned in a ventral-dorsal pattern, to reach their targets (Lehman et al. 2011). Ultimately, fibers from the medial portions of the OFC and PFC were found to travel ventral to fibers from the lateral portions of the OFC (Lehman et al. 2011). A subsequent study used probabilistic tractography to re-demonstrate these findings regarding the cOFC and lOFC in small numbers of both macaques and humans, though with some technical challenges in replicating vmPFC tracer data (Jbabdi et al. 2013).

Our study builds upon these data by using a different tractography algorithm and by including analysis of the mOFC in a large number of patients. Ultimately, our method allowed us to show these organizational rules are clearly maintained in the mOFC, cOFC, and lOFC. In addition, our center-of-mass analysis allowed further consolidation and refinement of these tracts to illustrate better the spatial properties of these tracts and to define them as belonging to the anterior thalamic radiations (OFC-SCT-thalamus) and to the medial forebrain bundle (OFC-SCT-brainstem). Deterministic tractography may be more conservative in visualizing connecting tracts while probabilistic tractography may leak into unexpected regions (Moldrich et al. 2010; Qazi et al. 2009). In addition, our correlation with anatomical primate data further strengthens the elucidated fiber connections. Importantly, our approach, which uses clinical data rather than simulation (Schoene-Bake et al. 2010), shows the clinical relevance of the anatomical organization of these fiber tracts involved in OCD.

Deep brain stimulation has been used with success for OCD, with recent studies indicating that it improves overall quality of life (Ooms et al. 2014). One of the commonly used targets includes the ventral capsule/ventral striatum (VC/VS), which affects an area that includes the nucleus accumbens (Blomstedt et al. 2013; de Koning et al. 2011). The topographic pattern by which different parts of the OFC reach their targets in the thalamus and brainstem has implications for the VC/VS DBS site, as the organization of traveling fibers implies that stimulation of specific tracts can be modulated by examining the spatial characteristics of each electrode contact (Lehman et al. 2011). This region is similar to that affected by SCT, and our data further support the idea that differential fiber tracts that are connected to subsections of the OFC could potentially be activated by selective DBS programming.

Based on the organization of the traveling mOFC and lOFC fibers, the use of SCT for treatment of medically resistant OCD reinforces the role of these structures in psychopathology. Furthermore, our previous pilot study (Yang et al. 2014), which sought to understand better how lesion placement and morphometry could be related to clinical outcome, suggested that SCT lesions placed more posteroventrally tended to have more positive clinical outcome. Applied to the current study, this would suggest that modulation of the more ventral tracts from the mOFC would lead to better outcome, which is in line with animal model studies. However, given that the prior study that sought to link lesion analysis and clinical outcome was a pilot investigation, these results should be considered tentative.

Limitations of this work include the use of healthy volunteers for understanding white matter tract involvement in the SCT lesion; one study has suggested diffuse white matter changes in patients with OCD (Jayarajan et al. 2012). Another limitation of this study is its basis in tractography, as diffusion data are representative only of extracellular diffusion patterns rather than definitive anatomic tracts. Nevertheless, we have undertaken a large study of 60 patients to support our findings and have utilized a technique that accounts for crossing fibers as well as branching patterns. Overall, this dataset is robust and provides strong evidence that tracts connecting the mOFC, cOFC, and lOFC with the thalamus or brainstem are affected in SCT.

Conclusion

Subcaudate tractotomy is an effective neurosurgical procedure for the treatment of medically intractable OCD. Using multi-tensor tractography, tracts that connect with the mOFC, cOFC, lOFC were found to travel through the SCT lesion, providing more evidence of their involvement in OCD psychopathology. The patient-derived SCT lesion ROI provides a clinical context for the tractography data, which has not been done in prior studies. These tracts follow particular orientation as they connect with either the thalamus or brainstem – via the anterior thalamic radiations and medial forebrain bundle, respectively – suggesting that differential modulation of these tracts is possible and may have implications in making the SCT procedure more efficacious and in developing unique DBS programming paradigms.

Supplementary Material

Refer to Web version on PubMed Central for supplementary material.

Acknowledgments

Funding Sources: R01DA027804 (NM), R21EB016449 (NM)

References

Adler CM, McDonough-Ryan P, Sax KW, Holland SK, Arndt S, Strakowski SM. fMRI of neuronal activation with symptom provocation in unmedicated patients with obsessive compulsive disorder. Journal of Psychiatric Research. 2000; 34(5):317–324. [PubMed: 11104844]

Ahmari SE, Spellman T, Douglass NL, Kheirbek MA, Simpson HB, Deisseroth K, et al. Repeated cortico-striatal stimulation generates persistent OCD-like behavior. Science. 2013; 340(6137):1234–1239. [PubMed: 23744948]

An X, Bandler R, Ongür D, Price JL. Prefrontal cortical projections to longitudinal columns in the midbrain periaqueductal gray in macaque monkeys. The Journal of Comparative Neurology. 1998; 401(4):455–479. [PubMed: 9826273]

Ardekani S, Sinha U. Geometric distortion correction of high-resolution 3 T diffusion tensor brain images. Magnetic Resonance in Medicine. 2005; 54(5):1163–1171. [PubMed: 16187289]

Avants BB, Epstein CL, Grossman M, Gee JC. Symmetric diffeomorphic image registration with cross-correlation: evaluating automated labeling of elderly and neurodegenerative brain. Medical Image Analysis. 2008; 12(1):26–41. [PubMed: 17659998]

Barbas H, Henion TH, Dermon CR. Diverse thalamic projections to the prefrontal cortex in the rhesus monkey. The Journal of Comparative Neurology. 1991; 313(1):65–94. [PubMed: 1761756]

Bari A, Robbins TW. Inhibition and impulsivity: Behavioral and neural basis of response control. Progress in Neurobiology. 2013; 108:44–79. [PubMed: 23856628]

Baxter LR, Schwartz JM, Bergman KS, Szuba MP, Guze BH, Mazziotta JC, et al. Caudate glucose metabolic rate changes with both drug and behavior therapy for obsessive-compulsive disorder. Archives of General Psychiatry. 1992; 49(9):681–689. [PubMed: 1514872]

Beucke JC, Sepulcre J, Talukdar T, Linnman C, Zschenderlein K, Endrass T, et al. Abnormally high degree connectivity of the orbitofrontal cortex in obsessive-compulsive disorder. JAMA Psychiatry. 2013; 70(6):619–629. [PubMed: 23740050]

Blomstedt P, Sjöberg RL, Hansson M, Bodlund O, Hariz MI. Deep brain stimulation in the treatment of obsessive-compulsive disorder. World Neurosurgery. 2013; 80(6):e245–e253. [PubMed: 23044000]

Bos J, Benevento LA. Projections of the medial pulvinar to orbital cortex and frontal eye fields in the rhesus monkey (Macaca mulatta). Experimental Neurology. 1975; 49(2):487–496. [PubMed: 811490]

Bourne SK, Eckhardt CA, Sheth SA, Eskandar EN. Mechanisms of deep brain stimulation for obsessive compulsive disorder: effects upon cells and circuits. Frontiers in Integrative Neuroscience. 2012; 6:29–29. [PubMed: 22712007]

Bourne SK, Sheth SA, Neal J, Strong C, Mian MK, Cosgrove GR, et al. Beneficial effect of subsequent lesion procedures after nonresponse to initial cingulotomy for severe, treatment-refractory obsessive-compulsive disorder. Neurosurgery. 2013; 72(2):196–202. [PubMed: 23147780]

Braber, den A.; van 't,Ent, D.; Cath, DC.; Wagner, J.; Boomsma, DI.; de Geus, EJC. Brain activation during cognitive planning in twins discordant or concordant for obsessive-compulsive symptoms. Brain. 2010; 133(10):3123–3140. [PubMed: 20823085]

Breiter HC, Rauch SL, Kwong KK, Baker JR, Weisskoff RM, Kennedy DN, et al. Functional Magnetic Resonance Imaging of Symptom Provocation in Obsessive-Compulsive Disorder. Archives of General Psychiatry. 1996; 53(7):595–606. [PubMed: 8660126]

Bridges PK, Bartlett JR, Hale AS, Poynton AM, Malizia AL, Hodgkiss AD. Psychosurgery: stereotactic subcaudate tractomy. An indispensable treatment. The British Journal of Psychiatry. 1994; 165(5):599–611. [PubMed: 7866675]

Burguière E, Monteiro P, Feng G, Graybiel AM. Optogenetic stimulation of lateral orbitofronto-striatal pathway suppresses compulsive behaviors. Science. 2013; 340(6137):1243–1246. [PubMed: 23744950]

Cavada C, Compañy T, Tejedor J, Cruz-Rizzolo RJ, Reinoso-Suárez F. The anatomical connections of the macaque monkey orbitofrontal cortex. A review. Cerebral Cortex. 2000; 10(3):220–242. [PubMed: 10731218]

Caviness VS Jr, Meyer J, Makris N, Kennedy DN. MRI-based topographic parcellation of human neocortex: an anatomically specified method with estimate of reliability. Journal of Cognitive Neuroscience. 1996; 8(6):566–587. [PubMed: 23961985]

Coenen VA, Panksepp J, Hurwitz TA, Urbach H, Mädler B. Human medial forebrain bundle (MFB) and anterior thalamic radiation (ATR): imaging of two major subcortical pathways and the dynamic balance of opposite affects in understanding depression. The Journal of Neuropsychiatry and Clinical Neurosciences. 2012; 24(2):223–236. [PubMed: 22772671]

Coenen VA, Schlaepfer TE, Maedler B, Panksepp J. Cross-species affective functions of the medial forebrain bundle-implications for the treatment of affective pain and depression in humans. Neuroscience and Biobehavioral Reviews. 2011; 35(9):1971–1981. [PubMed: 21184778]

de Koning PP, Figee M, van den Munckhof P, Schuurman PR, Denys D. Current status of deep brain stimulation for obsessive-compulsive disorder: a clinical review of different targets. Current Psychiatry Reports. 2011; 13(4):274–282. [PubMed: 21505875]

Dougherty DD, Baer L, Cosgrove GR, Cassem EH, Price BH, Nierenberg AA, et al. Prospective long-term follow-up of 44 patients who received cingulotomy for treatment-refractory obsessive-compulsive disorder. American Journal of Psychiatry. 2002; 159(2):269–275. [PubMed: 11823270]

Feldman RP, Alterman RL, Goodrich JT. Contemporary psychosurgery and a look to the future. Journal of Neurosurgery. 2001; 95(6):944–956. [PubMed: 11765838]

Filipek PA, Richelme C, Kennedy DN, Caviness VS. The young adult human brain: an MRI-based morphometric analysis. Cerebral Cortex. 1994; 4(4):344–360. [PubMed: 7950308]

Frankle WG, Laruelle M, Haber SN. Prefrontal cortical projections to the midbrain in primates: evidence for a sparse connection. Neuropsychopharmacology. 2006; 31(8):1627–1636. [PubMed: 16395309]

Greenberg BD, Rauch SL, Haber SN. Invasive circuitry-based neurotherapeutics: stereotactic ablation and deep brain stimulation for OCD. Neuropsychopharmacology. 2010; 35(1):317–336. [PubMed: 19759530]

Haber SN, Brucker JL. Cognitive and limbic circuits that are affected by deep brain stimulation. Frontiers in Bioscience. 2009; 14:1823–1834.

Hodgkiss AD, Malizia AL, Bartlett JR, Bridges PK. Outcome after the psychosurgical operation of stereotactic subcaudate tractotomy, 1979–1991. The Journal of Neuropsychiatry and Clinical Neurosciences. 1995; 7(2):230–234. [PubMed: 7626968]

Hoexter MQ, Miguel EC, Diniz JB, Shavitt RG, Busatto GF, Sato JR. Predicting obsessive-compulsive disorder severity combining neuroimaging and machine learning methods. Journal of Affective Disorders. 2013; 150(3):1213–1216. [PubMed: 23769292]

Hou J, Wu W, Lin Y, Wang J, Zhou D, Guo J, et al. Localization of cerebral functional deficits in patients with obsessive-compulsive disorder: a resting-state fMRI study. Journal of Affective Disorders. 2012; 138(3):313–321. [PubMed: 22331021]

Jayarajan RN, Venkatasubramanian G, Viswanath B, Janardhan Reddy YC, Srinath S, Vasudev MK, Chandrashekar CR. White matter abnormalities in children and adolescents with obsessive-compulsive disorder: a diffusion tensor imaging study. Depression and Anxiety. 2012; 29(9):780–788. [PubMed: 22323419]

Jbabdi S, Lehman JF, Haber SN, Behrens TE. Human and monkey ventral prefrontal fibers use the same organizational principles to reach their targets: tracing versus tractography. The Journal of Neuroscience. 2013; 33(7):3190–3201. [PubMed: 23407972]

Jung HH, Kim C-H, Chang JH, Park YG, Chung SS, Chang JW. Bilateral Anterior Cingulotomy for Refractory Obsessive-Compulsive Disorder: Long-Term Follow-Up Results. Stereotactic and Functional Neurosurgery. 2006; 84(4):184–189. [PubMed: 16912517]

Kelly D, Richardson A, Mitchell-Heggs N. Stereotactic limbic leucotomy: neurophysiological aspects and operative technique. The British Journal of Psychiatry. 1973; 123(573):133–140. [PubMed: 4582234]

Kievit J, Kuypers HG. Organization of the thalamo-cortical connexions to the frontal lobe in the rhesus monkey. Experimental Brain Research. 1977; 29(4):299–322. [PubMed: 410652]

Knight GC. Bi-frontal Stereotactic Tractotomy: An Atraumatic Operation of Value in the Treatment of Intractable Psychoneurosis: Part: I Anatomical and Surgical Observations. The British Journal of Psychiatry. 1969; 115(520):257–266. [PubMed: 4893673]

Lehman JF, Greenberg BD, McIntyre CC, Rasmussen SA, Haber SN. Rules ventral prefrontal cortical axons use to reach their targets: implications for diffusion tensor imaging tractography and deep brain stimulation for psychiatric illness. The Journal of Neuroscience. 2011; 31(28):10392–10402. [PubMed: 21753016]

Leiphart JW, Valone FH. Stereotactic lesions for the treatment of psychiatric disorders. Journal of Neurosurgery. 2010; 113(6):1204–1211. [PubMed: 20560726]

Makris N, Meyer JW, Bates JF, Yeterian EH, Kennedy DN, Caviness VS. MRI-Based topographic parcellation of human cerebral white matter and nuclei II. Rationale and applications with systematics of cerebral connectivity. NeuroImage. 1999; 9(1):18–45. [PubMed: 9918726]

Makris N, Preti MG, Wassermann D, Rathi Y, Papadimitriou GM, Yergatian C, et al. Human middle longitudinal fascicle: segregation and behavioral-clinical implications of two distinct fiber connections linking temporal pole and superior temporal gyrus with the angular gyrus or superior parietal lobule using multi-tensor tractography. Brain Imaging and Behavior. 2013; 7(3):335–352. [PubMed: 23686576]

Malcolm JG, Shenton ME, Rathi Y. Filtered multitensor tractography. IEEE Transactions on Medical Imaging. 2010; 29(9):1664–1675. [PubMed: 20805043]

Mashour GA, Walker EE, Martuza RL. Psychosurgery: past, present, and future. Brain Research. 2005; 48(3):409–419. [PubMed: 15914249]

McGuire PK, Bench CJ, Frith CD, Marks IM, Frackowiak RS, Dolan RJ. Functional anatomy of obsessive-compulsive phenomena. The British Journal of Psychiatry. 1994; 164(4):459–468. [PubMed: 8038933]

Meyer JW, Makris N, Bates JF, Caviness VS, Kennedy DN. MRI-Based topographic parcellation of human cerebral white matter. NeuroImage. 1999; 9(1):1–17. [PubMed: 9918725]

Moldrich RX, Pannek K, Hoch R, Rubenstein JL, Kurniawan ND, Richards LJ. Comparative mouse brain tractography of diffusion magnetic resonance imaging. NeuroImage. 2010; 51(3):1027–1036. [PubMed: 20303410]

Nieuwenhuys, R.; Voogd, J.; van Huijzen, C. The Human Central Nervous System: A Synopsis and Atlas. Third Edition. New York: Springer-Verlag; 1988.

Nieuwenhuys, R.; Voogd, J.; van Huijzen, C. The Human Central Nervous System. Fourth Edition.. New York: Springer; 2008.

Ooms P, Mantione M, Figee M, Schuurman PR, van den Munckhof P, Denys D. Deep brain stimulation for obsessive-compulsive disorders: long-term analysis of quality of life. Journal of Neurology, Neurosurgery & Psychiatry. 2014; 85(2):153–158.

Pallanti S, Quercioli L. Treatment-refractory obsessive-compulsive disorder: methodological issues, operational definitions and therapeutic lines. Progress in Neuro- Psychopharmacology& Biological Psychiatry. 2006; 30(3):400–412. [PubMed: 16503369]

Paxinos, G.; Huang, X-F. Atlas of the Human Brainstem. Boston: Academic Press; 1995.

Perani D, Colombo C, Bressi S, Bonfanti A, Grassi F, Scarone S, et al. [18F]FDG PET study in obsessive-compulsive disorder. A clinical/metabolic correlation study after treatment. The British Journal of Psychiatry. 1995; 166(2):244–250. [PubMed: 7728370]

Piras F, Piras F, Chiapponi C, Girardi P, Caltagirone C, Spalletta G. Widespread structural brain changes in OCD: A systematic review of voxel-based morphometry studies. CORTEX. 2013

Poellinger A, Thomas R, Lio P, Lee A, Makris N, Rosen BR, Kwong KK. Activation and Habituation in Olfaction—An fMRI Study. NeuroImage. 2001; 13(4):547–560. [PubMed: 11305885]

Porrino LJ, Goldman-Rakic PS. Brainstem innervation of prefrontal and anterior cingulate cortex in the rhesus monkey revealed by retrograde transport of HRP. The Journal of Comparative Neurology. 1982; 205(1):63–76. [PubMed: 6121826]

Qazi AA, Radmanesh A, O'Donnell L, Kindlmann G, Peled S, Whalen S, et al. Resolving crossings in the corticospinal tract by two-tensor streamline tractography: Method and clinical assessment using fMRI. NeuroImage. 2009; 47(Suppl 2):T98–T106. [PubMed: 18657622]

Rademacher J, Galaburda AM, Kennedy DN, Filipek PA, Caviness VS Jr. Human cerebral cortex: localization, parcellation, and morphometry with magnetic resonance imaging. Journal of Cognitive Neuroscience. 1992; 4(4):352–374. [PubMed: 23968129]

Rauch SL, Jenike MA, Alpert NM, Baer L, Breiter HCRSC, Fischman AJ. Regional Cerebral Blood Flow Measured During Symptom Provocation in Obsessive-Compulsive Disorder Using Oxygen 15—Labeled Carbon Dioxide and Positron Emission Tomography. Archives of General Psychiatry. 1994; 51(1):62–70. [PubMed: 8279930]

Ray JP, Price JL. The organization of projections from the mediodorsal nucleus of the thalamus to orbital and medial prefrontal cortex in macaque monkeys. The Journal of Comparative Neurology. 1993; 337(1):1–31. [PubMed: 7506270]

Romanski LM, Giguere M, Bates JF, Goldman-Rakic PS. Topographic organization of medial pulvinar connections with the prefrontal cortex in the rhesus monkey. The Journal of Comparative Neurology. 1997; 379(3):313–332. [PubMed: 9067827]

Rotge J-Y, Guehl D, Dilharreguy B, Cuny E, Tignol J, Bioulac B, et al. Provocation of obsessive-compulsive symptoms: a quantitative voxel-based meta-analysis of functional neuroimaging studies. Journal of Psychiatry & Neuroscience. 2008; 33(5):405–412. [PubMed: 18787662]

Rotge J-Y, Guehl D, Dilharreguy B, Tignol J, Bioulac B, Allard M, et al. Meta-analysis of brain volume changes in obsessive-compulsive disorder. Biological Psychiatry. 2009; 65(1):75–83. [PubMed: 18718575]

Rotge J-Y, Langbour N, Guehl D, Bioulac B, Jaafari N, Allard M, et al. Gray matter alterations in obsessive-compulsive disorder: an anatomic likelihood estimation metaanalysis. Neuropsychopharmacology. 2010a; 35(3):686–691. [PubMed: 19890260]

Rotge J-Y, Langbour N, Jaafari N, Guehl D, Bioulac B, Aouizerate B, et al. Anatomical alterations and symptom-related functional activity in obsessive-compulsive disorder are correlated in the lateral orbitofrontal cortex. Biological Psychiatry. 2010b; 67(7):e37–e38. [PubMed: 20015485]

Schoene-Bake J-C, Parpaley Y, Weber B, Panksepp J, Hurwitz TA, Coenen VA. Tractographic analysis of historical lesion surgery for depression. Neuropsychopharmacology. 2010; 35(13): 2553–2563. [PubMed: 20736994]

Schwartz JM, Stoessel PW, Baxter LR, Martin KM, Phelps ME. Systematic changes in cerebral glucose metabolic rate after successful behavior modification treatment of obsessive-compulsive disorder. Archives of General Psychiatry. 1996; 53(2):109–113. [PubMed: 8629886]

Swedo SE, Pietrini P, Leonard HL, Schapiro MB, Rettew DC, Goldberger EL, et al. Cerebral glucose metabolism in childhood-onset obsessive-compulsive disorder. Revisualization during pharmacotherapy. Archives of General Psychiatry. 1992; 49(9):690–694. [PubMed: 1514873]

Szeszko PR, Robinson D, Alvir JM, Bilder RM, Lencz T, Ashtari M, et al. Orbital frontal and amygdala volume reductions in obsessive-compulsive disorder. Archives of General Psychiatry. 1999; 56(10):913–919. [PubMed: 10530633]

Talairach, J.; Tournoux, P. Co-planar Stereotaxic Atlas of the Human Brain: 3-dimensional Proportional System. Thieme Medical Pub; 1988.

Trojanowski JQ, Jacobson S. Areal and laminar distribution of some pulvinar cortical efferents in rhesus monkey. The Journal of Comparative Neurology. 1976; 169(3):371–392. [PubMed: 823181]

Yang JC, Ginat DT, Dougherty DD, Makris N, Eskandar EN. Lesion analysis for cingulotomy and limbic leucotomy: comparison and correlation with clinical outcomes. Journal of Neurosurgery. 2014; 120(1):152–163. [PubMed: 24236652]

Yeterian EH, Pandya DN. Corticothalamic connections of paralimbic regions in the rhesus monkey. The Journal of Comparative Neurology. 1988; 269(1):130–146. [PubMed: 3361000]

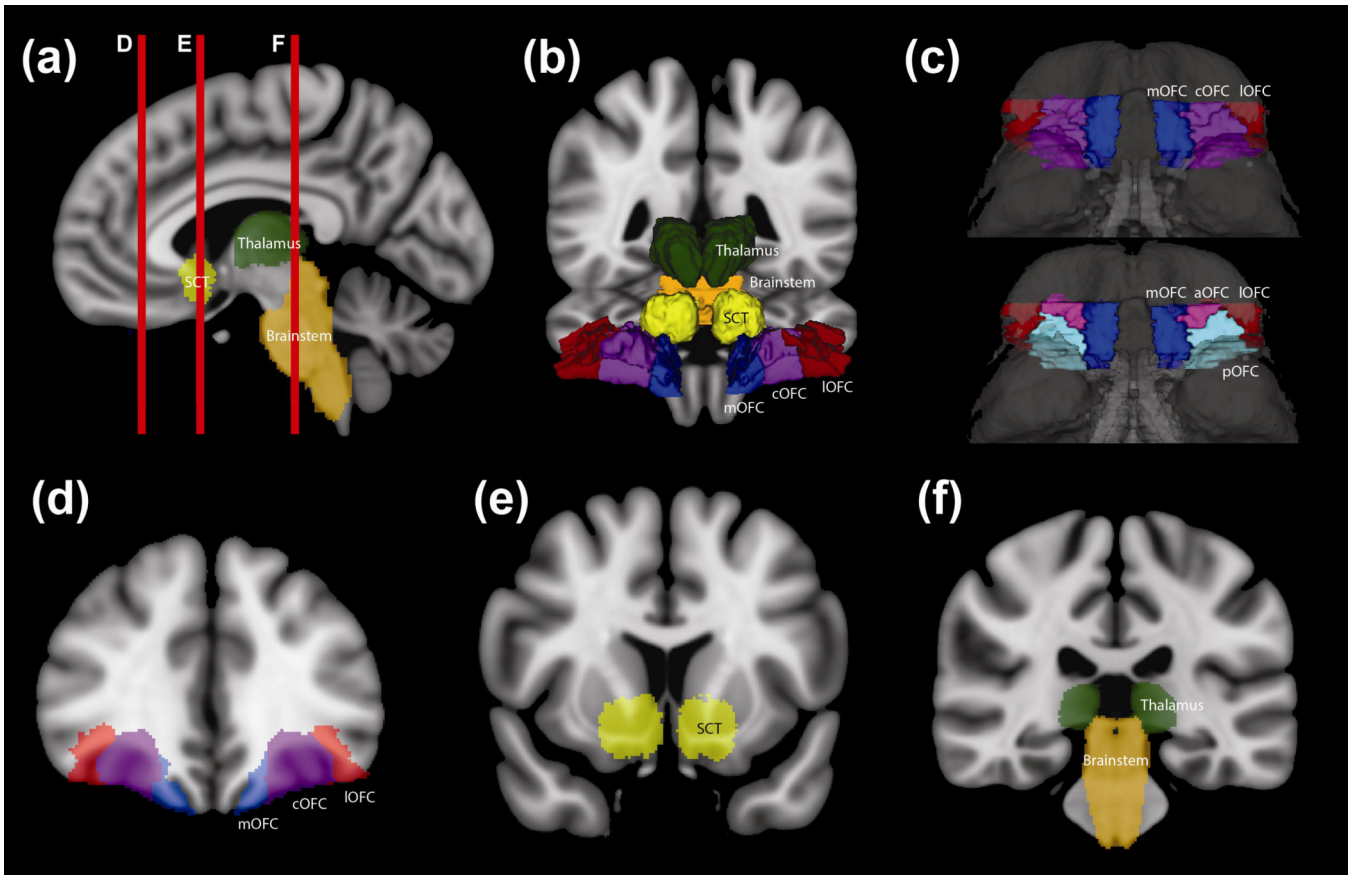

Fig. 1. Region of Interest (ROI) Definition

(a) Sagittal T1-weighted MNI152 brain with medial orbitofrontal cortex (mOFC, blue), subcaudate tractotomy lesion (SCT, yellow), thalamus (green), and brainstem (orange). Red vertical lines indicate the coronal sections in D, E, and F.

(b) 3D anterior projection of ROIs on T1-weighed MNI152 brain. In addition to (a), lateral orbitofrontal cortex (lOFC, red) and central orbitofrontal cortex (cOFC, purple) are shown.

(c) 3D projection of ventral surface of MNI12 brain, with mOFC (blue), cOFC (purple), and lOFC (red). For comparison, aOFC (pink) and pOFC (cyan) additionally shown.

(d) Coronal T1-weighted MNI152 brain with mOFC (blue), cOFC (purple), and lOFC (red)

(e) Coronal T1-weighted MNI152 brain with SCT (yellow)

(f) Coronal T1-weighted MNI152 brain with thalamus (green) and brainstem (orange)

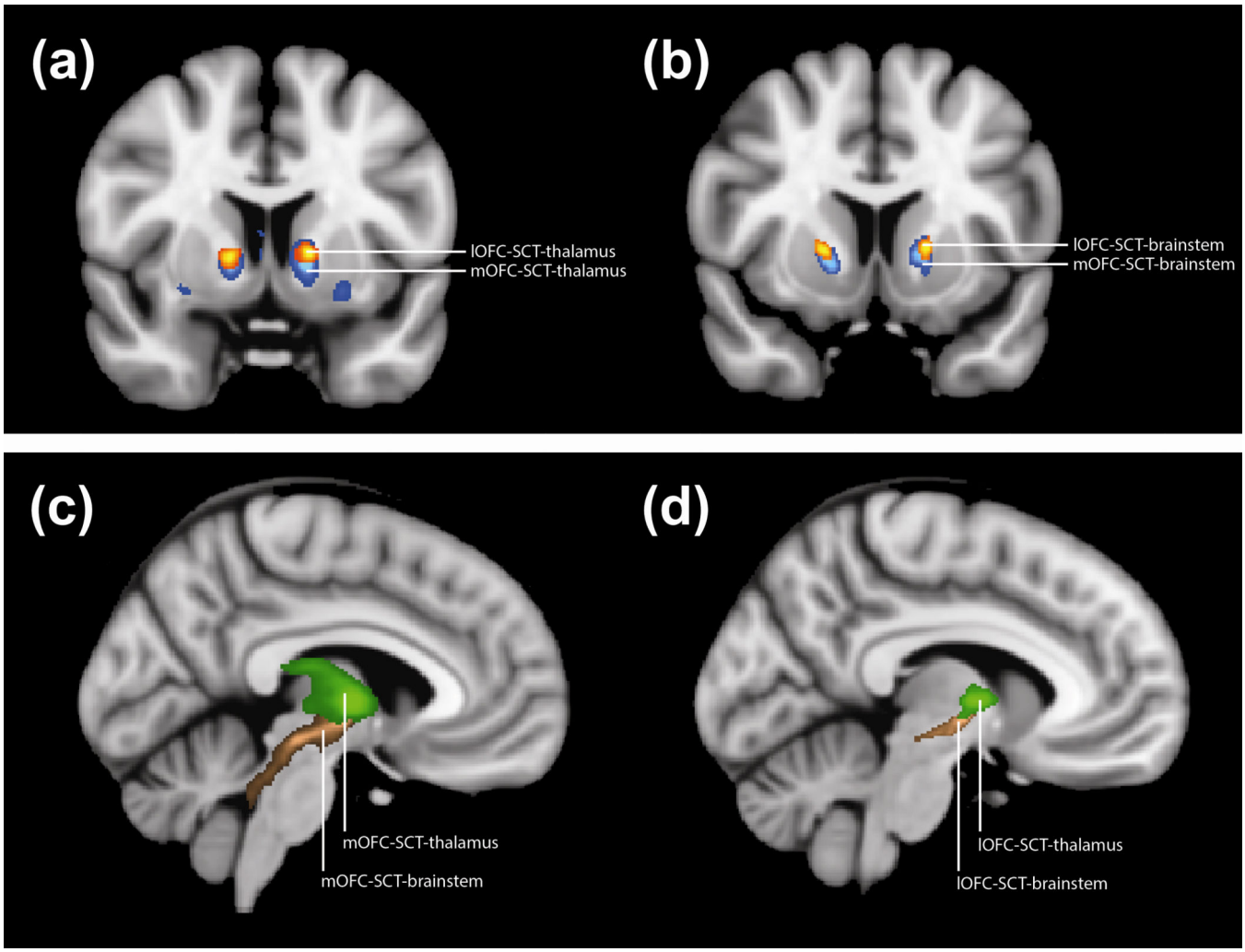

Fig. 2. Probability Maps of Fibers Traversing the SCT lesion

(a) Coronal T1-weighted MNI152 brain with probability map for fibers that connect thalamus to subcaudate tractotomy lesion (SCT) and medial orbitofrontal cortex (mOFC) (blue) or lateral orbitofrontal cortex (lOFC) (orange)

(b) Coronal T1-weighted MNI152 brain with probability map for fibers that connect brainstem to SCT and mOFC (blue) or lOFC (orange)

(c) Sagittal T1-weighted MNI152 brain with probability map for fibers that connect mOFC to thalamus (green) or brainstem (brown)

(d) Sagittal T1-weighted MNI152 brain with probability map for fibers that connect lOFC to thalamus (green) or brainstem (brown)

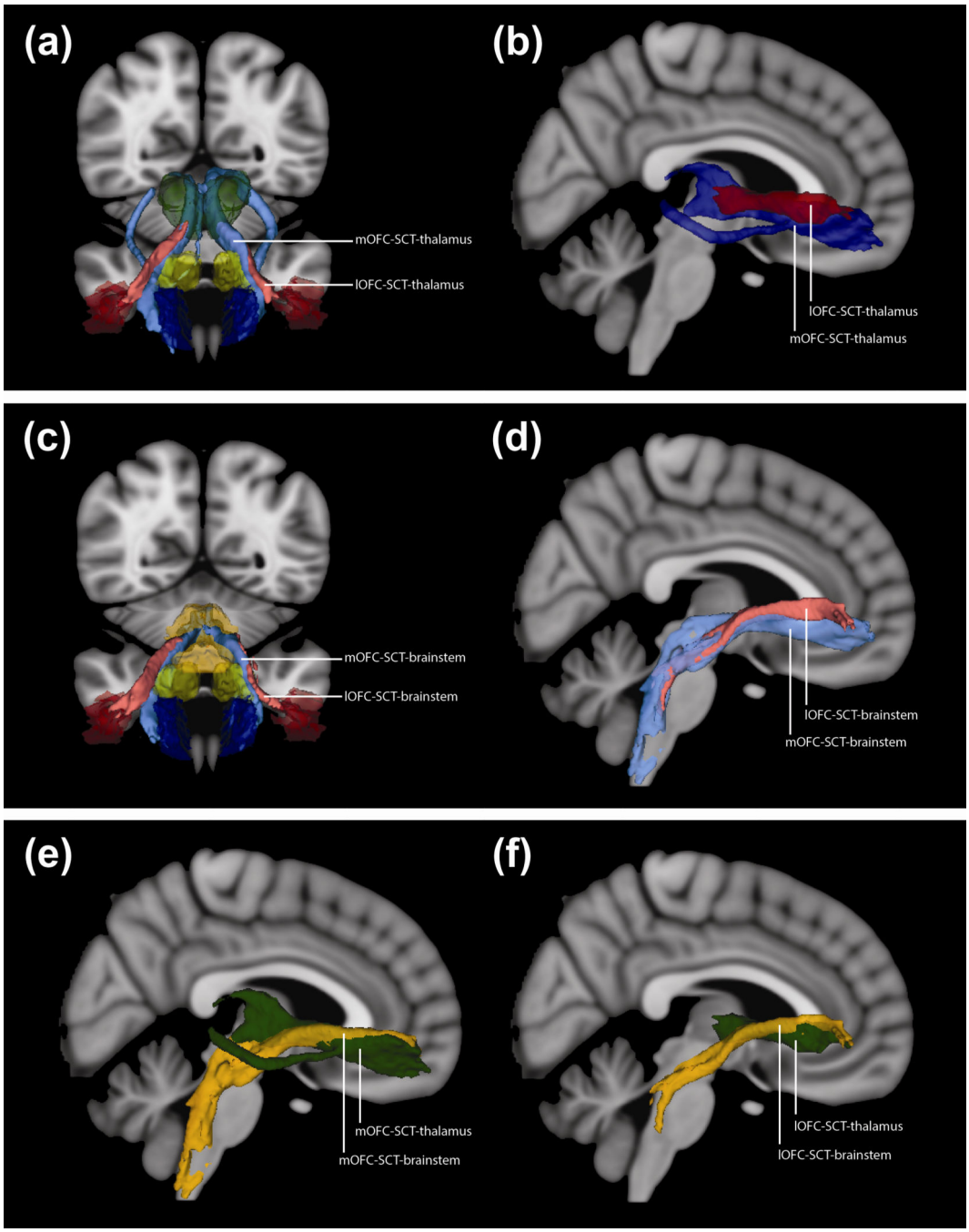

Fig. 3. 3D Projections of Fiber Tracts

(a) 3D anterior projection on T1-weighted MNI152 brain. ROIs: medial orbitofrontal cortex (mOFC, dark blue), lateral orbitofrontal cortex (lOFC, dark red), subcaudate tractotomy lesion (SCT, yellow), and thalamus (green). Blue tract connects mOFC, SCT, and thalamus; red tract connects lOFC, SCT, and thalamus.

(b) 3D right lateral projection of tracts on T1-weighted MNI152 brain. Dark blue tract connects mOFC, SCT, and thalamus; dark red tract connects lOFC, SCT, and thalamus. The central orbitofrontal cortex (cOFC) tract is not shown to facilitate visualization.

(c) 3D anterior projection on T1-weighted MNI152 brain. ROIs: mOFC (dark blue), lOFC (dark red), SCT (yellow), and brainstem (orange). Blue tract connects mOFC, SCT, and brainstem; red tract connects lOFC, SCT, and brainstem.
(d) 3D right lateral projection of tracts on T1-weighted MNI152 brain. Light blue tract connects mOFC, SCT, and brainstem; light red tract connects lOFC, SCT, and brainstem. The cOFC tract is not shown to facilitate visualization.
(e) 3D right lateral projection of tracts connected to mOFC on T1-weighted MNI152 brain. Green tract connects mOFC, SCT, and thalamus; orange tract connects mOFC, SCT, and brainstem.
(f) 3D right lateral projection of tracts connected to lOFC on T1-weighted MNI152 brain. Green tract connects lOFC, SCT, and thalamus; orange tract connects lOFC, SCT, and brainstem.

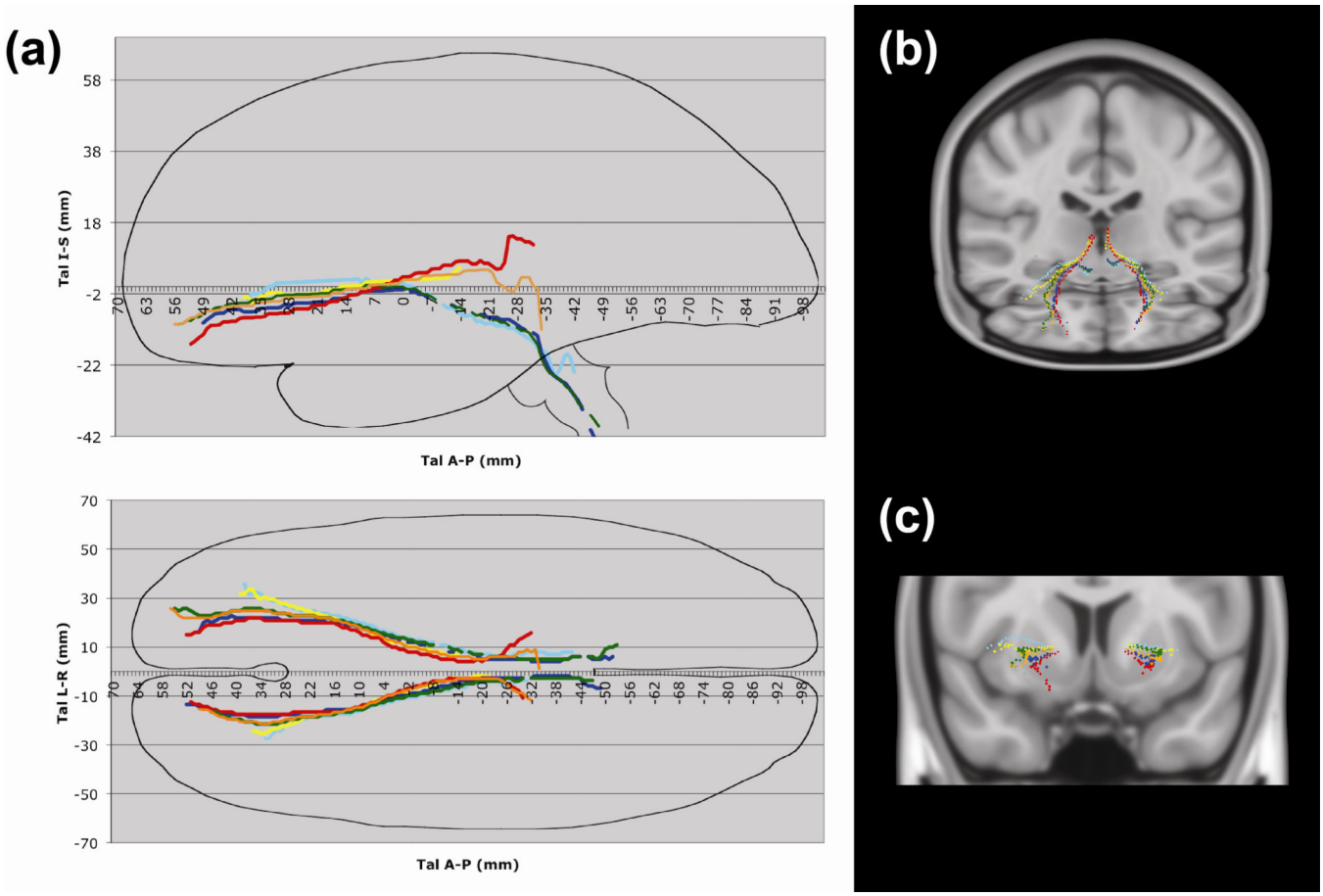

Fig. 4. Orbitofrontal Tracts Represented as Talairach Coordinates

(a) Right lateral and axial projections of tracts with approximate Talairach brain outline. The top graph is a right sagittal projection, with the Talairach anterior-posterior coordinate on the x-axis and the Talairach inferior-superior coordinate on the y-axis. The bottom graph is an axial projection, with the Talairach anterior-posterior coordinate on the x-axis and the Talairach right-left coordinate on the y-axis. These tracts run through the medial orbitofrontal cortex (mOFC), central orbitofrontal cortex (cOFC), or lateral orbitofrontal cortex (lOFC); subcaudate tractotomy lesion (SCT); and thalamus or brainstem. Tracts: mOFC-SCT-thalamus (red: fibers traveling through the internal capsule), mOFC-SCT-brainstem (blue), cOFC-SCT-thalamus (orange: fibers traveling through the internal capsule), cOFC-SCT-brainstem (green), lOFC-SCT-thalamus (yellow), and lOFC-SCT-brainstem (cyan).

(b) 3D oblique and C. coronal projections of tracts in Talairach space, using center-of-mass coordinates. Tracts: mOFC-SCT-thalamus (red: fibers traveling through the internal capsule), mOFC-SCT-brainstem (blue), cOFC-SCT-thalamus (orange: fibers traveling through the internalcapsule), cOFC-SCT-brainstem (green), lOFC-SCT-thalamus (yellow), and lOFC-SCT386 brainstem (cyan).

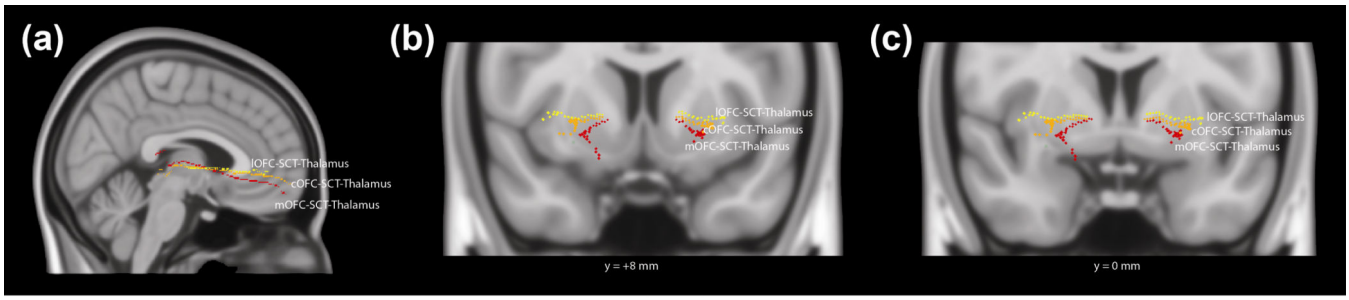

Fig. 5. 3D Projections of Talairach Coordinates for Orbitofrontal Cortex-Thalamus Tract

(a) 3D sagittal, (b) coronal (level of the nucleus accumbens, Talairach y-coordinate = +8mm), and (c) coronal (level of the anterior commissure, Talairach y-coordinate = 0mm) projections of tracts in Talairach space, using center-of-mass coordinates. These tracts run through the medial orbitofrontal cortex (mOFC), central orbitofrontal cortex (cOFC), or lateral orbitofrontal cortex (lOFC); subcaudate tractotomy lesion (SCT); and thalamus. Tracts: mOFC-SCT-thalamus (red: fibers traveling through the internal capsule), cOFC-SCT-thalamus (orange: fibers traveling through the internal capsule), and lOFC-SCT-thalamus (yellow).

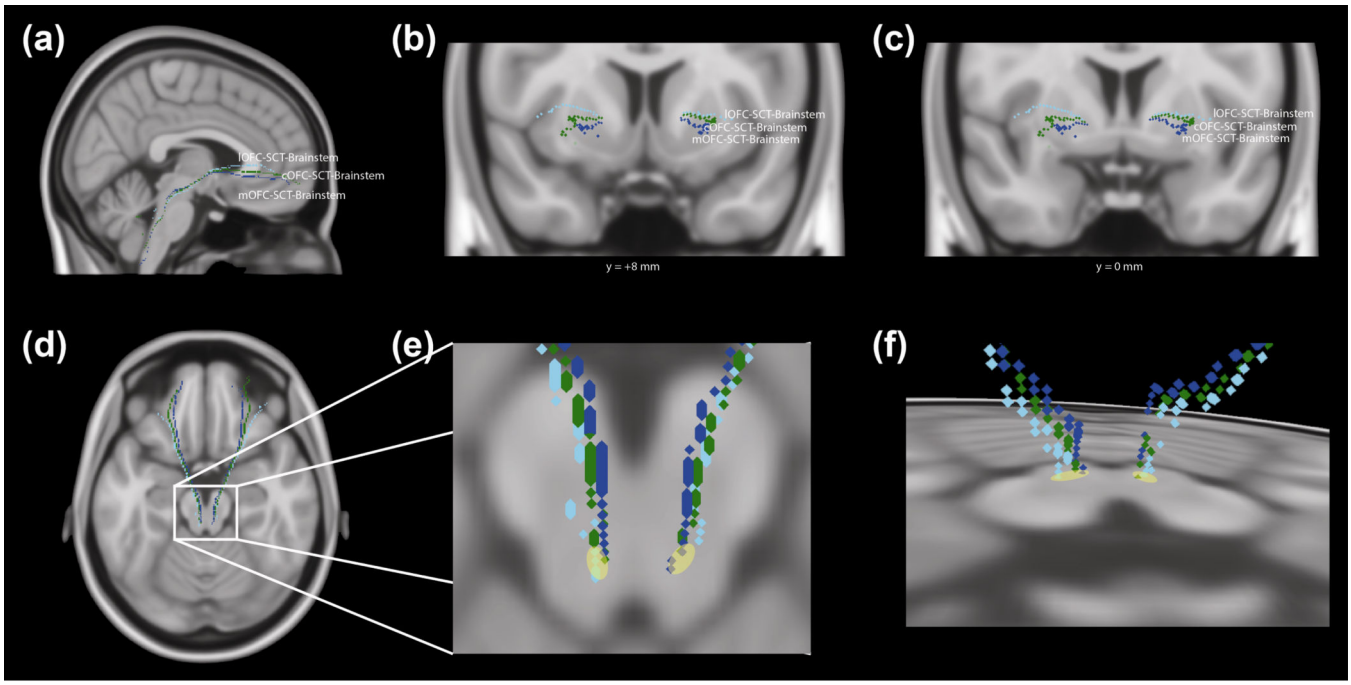

Fig. 6. 3D Projections of Talairach Coordinates for Orbitofrontal Cortex-Brainstem Tract

(a) 3D sagittal, (b) coronal (level of the nucleus accumbens, Talairach y-coordinate = +8mm), (c) coronal (level of the anterior commissure, Talairach y-coordinate = 0mm), and (d) axial projections of tracts in Talairach space, using center-of-mass coordinates. These tracts run through the medial orbitofrontal cortex (mOFC), central orbitofrontal cortex (cOFC), or lateral orbitofrontal cortex (lOFC); subcaudate tractotomy lesion (SCT); and brainstem. Tracts: mOFC403 SCT-brainstem (blue), cOFC-SCT-brainstem (green), and lOFC-SCT-brainstem (cyan). (e) Expanded region of brainstem of (d). The yellow region indicates the approximate area of intersection between the tracts and the axial slice. (f) 3D oblique projection of tracts in Talairach space, with a view from the dorsal aspect.